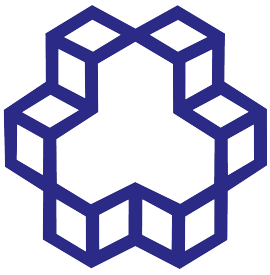

K. N. Toosi University
of Technology

Faculty of Mechanical Engineering

Final Project of Chassis Systems

Machine Learning Assisted Optimization of McPherson Suspension Kinematics Using Neural Networks and Quasi-Newton Methods

By

Amirhossein Mohammadi

Supervisor

Dr. Shahram Azadi

August 2025

Abstract

This report presents a comprehensive study on the optimization of McPherson suspension kinematics using machine learning and gradient-based methods. The project begins with full-vehicle dynamics simulations, including Single Lane Change and J-Turn maneuvers, to evaluate handling characteristics such as lateral velocity, roll angle, yaw rate, and side slip angle. Key findings highlight the significant role of the anti-roll bar in maintaining vehicle stability. The second phase focuses on optimizing the front McPherson suspension geometry through sensitivity analysis and Design of Experiments (DOE), identifying critical hard-points affecting camber, toe, and track width. A neural network model is trained to predict suspension behavior, and the L-BFGS-B optimization algorithm is employed to minimize deviations from target performance curves. The optimized design demonstrates improved camber gain, reduced understeer gradient, and enhanced track width stability, aligning closely with ideal kinematic behavior.

Keywords: McPherson suspension, vehicle dynamics, machine learning, neural networks, gradient-based optimization, camber angle, toe angle, track width, L-BFGS-B, ADAMS simulation, Python

Table of Contents

1. Introduction
1

1.1. Different Types of Suspension Systems
2

1.2. Kinematics and Elastokinematics of a Suspension System
4

1.3. Machine Learning: Basic Definitions
7

2. Full Vehicle Maneuvering Simulations
7

3. McPherson Suspension System Identification
17

3.1. Baseline Simulation
17

3.2. Sensitivity Analysis and Design of Experiments
20

4. Optimization using Neural Networks and Gradient Based Methods
23

4.1. Dataset Collection
23

4.2. Preprocessing
24

4.3. Model Training and Evaluation
24

4.4. Optimization
25

Conclusion
33

References
34

1. Introduction

Vehicle dynamics is the study of forces and motions governing the behavior of the vehicle. It bridges mechanics, control theory, and design to optimize and encompass several key domains. Some of the most important fundamental areas are as follows.

- Longitudinal Dynamics focuses on acceleration and braking performance, involving engine torque, aerodynamic drag, tire-road friction, and weight transfer during speed changes.
- Lateral Dynamics governs cornering behavior, handling stability, maneuvering, and steering response, influenced by suspension geometry, roll stiffness, and tire slip angles during turns.
- Tire Dynamics defines the interaction between tires and the road, determining grip, slip behavior, and force generation under braking, acceleration, and cornering.
- Vertical Dynamics deals with suspension performance, ride comfort, handling performance, and wheel control over uneven surfaces, optimizing spring-damper systems and kinematics like camber/toe curves.

Each domain interacts longitudinal forces affect tire grip, lateral motion depends on suspension tuning, and vertical dynamics influence tire contact making integrated optimization essential for balanced performance.

This report presents a comprehensive vehicle dynamics analysis in two parts. First, full vehicle handling simulations are conducted for an AWD sedan, evaluating performance through standardized Single Lane Change and J-Turn maneuvers. The second part focuses on front suspension system optimization, where the McPherson strut geometry is systematically refined in order to meet target performance specifications while maintaining packaging constraints.

1.1. Different Types of Suspension Systems

Modern vehicles employ three fundamental suspension types of dependent, independent (rigid), and semi-independent each offering distinct trade-offs between cost, comfort, and performance.

- Dependent (rigid) suspension systems, feature a solid axle that connects both wheels, causing them to move in unison exemplified by live axles with leaf springs as shown in Figure 1.1 or torque tubes (e.g., classic trucks). This design prioritizes durability and load-bearing capacity but compromises ride comfort and handling precision.

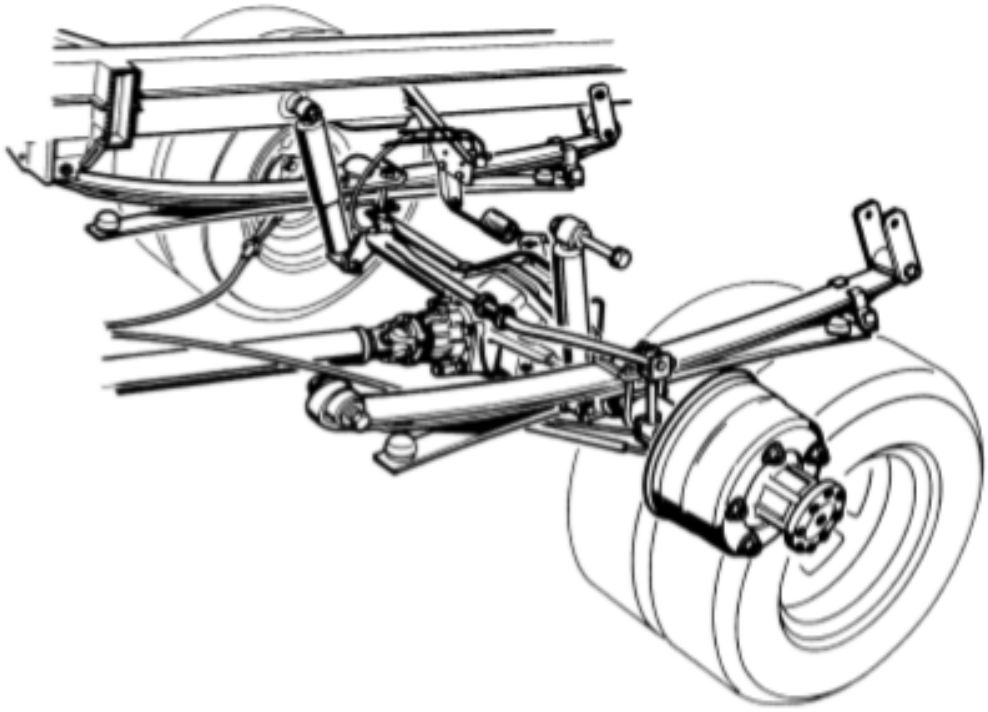

Figure 1.1. Rear Solid Axle of the VW LT Light Commercial Vehicle (Source: Jornsen Reimpell, Helmut Stoll, Jurgen W. Betzler, "The Automotive Chassis: Engineering Principles", Butterworth-Heinemann, 2001, Fig. 1.20)

- Independent suspension systems as shown in Figure 1.2 allow wheels to move separately via mechanisms like McPherson struts, double

wishbones, or multi-link arrangements, offering superior handling and traction at higher cost.

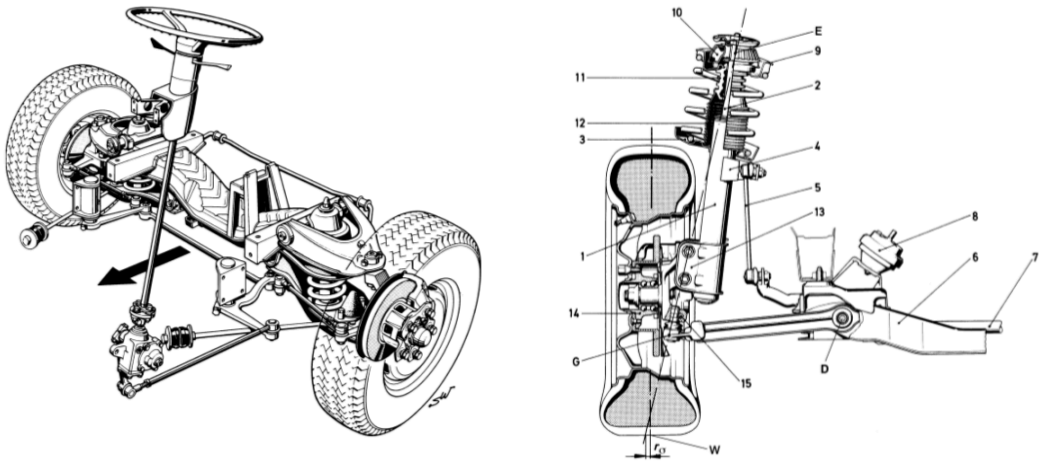

Figure 1.2. Double Wishbone Front Axle on the VW Light Commercial Vehicle and Rear View of the Left-Hand Side of the McPherson Front Axle on the Opel Omega (1999) (Source: Jornsen Reimpell, Helmut Stoll, Jurgen W. Betzler, “The Automotive Chassis: Engineering Principles”, Butterworth-Heinemann, 2001, Fig. 1.7 and Fig. 1.8)

- Semi-independent suspensions bridge the gap with designs like torsion beams or twist axles (Figure 1.3), where a flexible cross-member permits limited independent movement, balancing affordability with adequate comfort. From heavy-duty solid axles to performance-tuned multi-link setups, each architecture serves distinct needs, reflecting trade-offs in cost, complexity, and dynamic performance.

Figure 1.3. Twist-beam suspension of the VW Golf IV (1997), VW Bora (1999) and Audi A3 (1996) (Source: Jornsen Reimpell, Helmut Stoll, Jurgen W. Betzler, “The Automotive Chassis: Engineering Principles”, Butterworth-Heinemann, 2001, Fig. 1.7 and Fig. 1.8)

1.2. Kinematics and Elastokinematics of a Suspension System

Kinematics refers to the motion of the wheels during vertical suspension travel and steering, often termed wheel or suspension geometry in standards such as DIN. In contrast, elastokinematics describes shifts in wheel position caused by forces and moments acting between the tires and the road, as well as longitudinal wheel displacement relative to suspension mounting points. These variations arise due to elastic deformation in suspension components, which helps manage compliance while maintaining kinematic integrity.

Design of a suspension system is mainly done through configuration and alteration of the design parameters affecting kinematics and elastokinematics. The performance specifications (design criteria) of a suspension system are quantified through kinematic and compliance curves, which describe the relationship between wheel travel and critical alignment parameters. The primary objective of this project is to optimize the hard-point geometry (key joint coordinates) of a McPherson strut suspension system to satisfy three essential performance targets mentioned as follows.

Camber angle variation refers to the change in the vertical tilt of the wheel (inward or outward) as the suspension moves through its travel range. During cornering, optimal camber behavior is critical - engineers typically design for progressive negative camber gain (wheels tilting inward) as the suspension compresses (bump) which can be seen in Figure 1.4. This design maximizes the tire contact patch when cornering forces are highest, improving grip. The camber curve is primarily determined by the strut top mount position (both vertically and laterally) and the geometry of the lower control arm. Performance vehicles often show more aggressive camber gain compared to comfort-oriented vehicles, demonstrating the tuning flexibility of these hard-points.

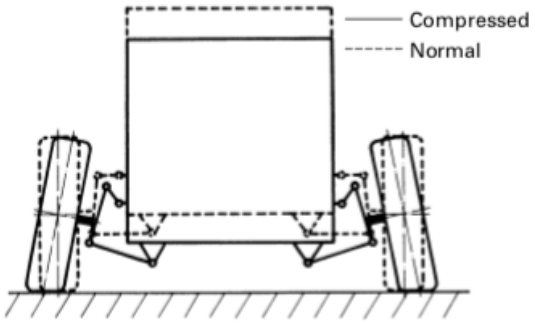

Figure 1.4. Negative Camber in Bump (Source: Jornsen Reimpell, Helmut Stoll, Jurgen W. Betzler, “The Automotive Chassis: Engineering Principles”, Butterworth-Heinemann, 2001, Fig. 3.47)

Toe angle progression describes how the wheel steering alignment (toe-in or toe-out) changes during suspension movement. Ideal designs maintain minimal toe variation during normal travel (within ±10 degrees) to ensure straight-line stability, while sometimes incorporating slight dynamic toe-in during braking for enhanced stability. The tie-rod linkage plays a crucial role - its length and attachment point on the steering knuckle significantly affect toe behavior. Additionally, the lateral compliance of control arm bushings influences how much toe change occurs under load.

This parameter requires careful balancing, as excessive toe variation can lead to nervous handling or accelerated tire wear.

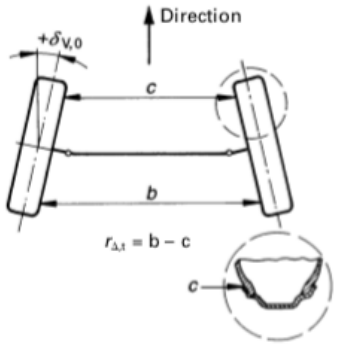

Figure 1.5. Toe-in Configuration (Source: Jornsen Reimpell, Helmut Stoll, Jurgen W. Betzler, “The Automotive Chassis: Engineering Principles”, Butterworth-Heinemann, 2001, Fig. 3.58)

Track width alteration measures the lateral displacement of wheels during suspension articulation. Excessive track width change causes tire scrub, reducing efficiency and causing uneven wear. This parameter is governed by the wheel center movement arc, which depends on control arm length and angle relative to the chassis. The suspension chassis mounting points are equally critical and their strategic placement ensures the wheel moves vertically with minimal side-to-side deviation. Proper control of track width alteration contributes significantly to predictable handling and consistent tire contact with the road surface.

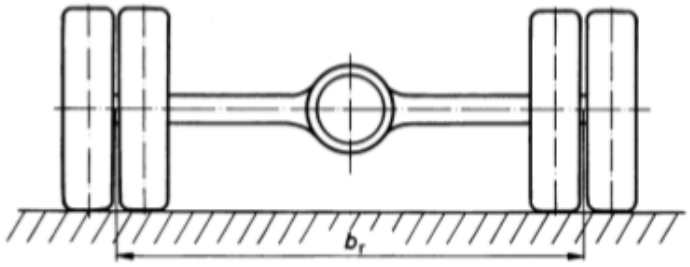

Figure 1.6. The Track Specification b_r Relates to The Mean Distance (Source: Jornsen Reimpell, Helmut Stoll, Jurgen W. Betzler, “The Automotive Chassis: Engineering Principles”, Butterworth-Heinemann, 2001, Fig. 3.4)

1.3. Machine Learning: Basic Definitions

Machine Learning (ML) is a transformative branch of Artificial Intelligence (AI) that focuses on developing self-improving algorithms and statistical models capable of performing complex tasks without being explicitly programmed. At its core, ML systems autonomously extract patterns from data, build mathematical representations of real-world processes, and make data-driven decisions that improve with experience. This adaptive learning capability distinguishes ML from traditional programming and makes it indispensable for modern applications ranging from computer vision and natural language processing to predictive maintenance and autonomous decision-making systems.

Fundamentally, machine learning provides a methodological framework for creating intelligent systems that learn directly from data. Data scientists and ML engineers employ these techniques to construct models that not only analyze and interpret complex datasets but also generate actionable predictions. The discipline sits at the intersection of computer science, statistics, and domain-specific knowledge, requiring careful consideration of both algorithmic theory and practical implementation.

2. Full Vehicle Maneuvering Simulations

As mentioned in the previous chapter, full vehicle handling simulations are conducted for an AWD sedan in MSC ADMAS software, evaluating performance through standardized Single Lane Change and J-Turn maneuvers.

Single Lane Change is a standardized maneuver where a vehicle quickly shifts to an adjacent lane at constant speed (typically 80-100 km/h) to test lateral stability (yaw rate/roll angle), steering response and path tracking accuracy.

J-Turn on the other hand is an aggressive 90° turn at high speed (e.g., 60 km/h) to evaluate transient handling during rapid direction change, weight transfer effects and electronic stability control (ESC) performance.

Both of these tests are ISO/SAE standardized tests for vehicle dynamics validation. The lane change assesses stability, while the J-turn stresses extreme handling limits.

The first phase of the project requires assembling a full AWD Sedan vehicle model in ADAMS software. As shown in Figure 2.1, all subsystems are properly defined. The suspension system includes an anti-roll bar in the front axle of the full vehicle model.

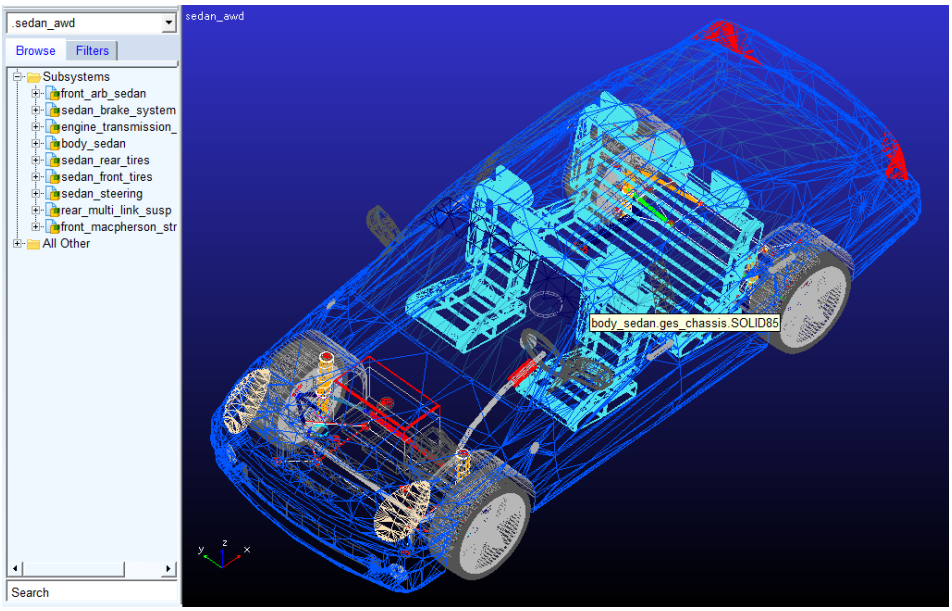

Figure 2.1. Full AWD Sedan Model and its Subsystems

Additionally, the tie rod components are being flexible and meshed (material: steel) to enable finite element analysis (FEA) as shown in Figure 2.2. This setup allow for structural and dynamic simulations in subsequent analysis stages.

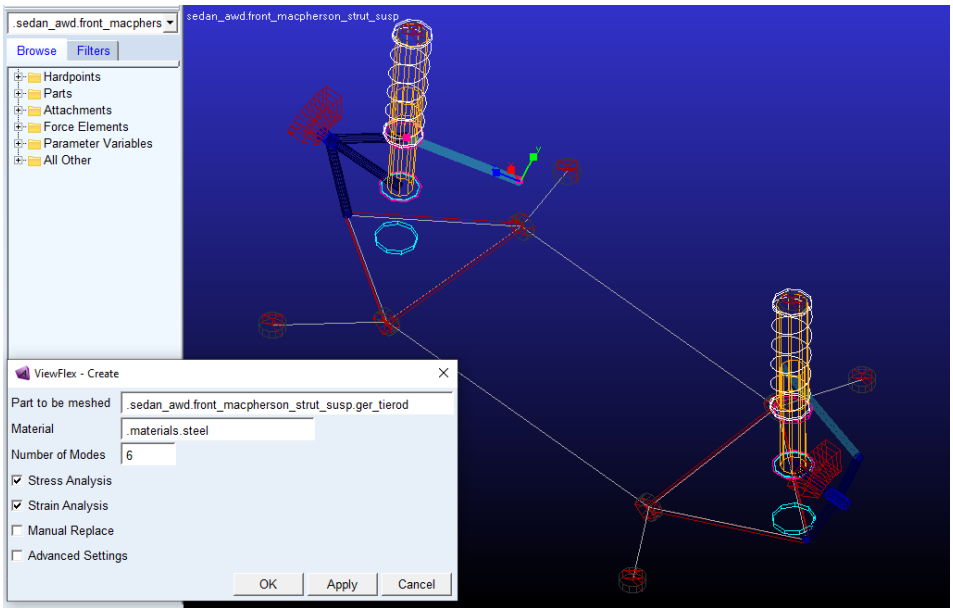

Figure 2.2. Full AWD Sedan Model and its Subsystems

In the next step and after meshing and replacing the tie rod components with the generated MNF files, the following dynamic analyses (Single Lane Change and J-Turn) on the complete AWD Sedan model are performed in ADAMS. Table 2.1 shows key parameter values used in the simulations.

Table 2.1. Handling Simulations Parameters

Parameter	**Single Lane Change**	**J-Turn**
Duration (s)	10	5
Number of steps	1000	500
Velocity (km/h)	80	80
Gear Position	4	4
Angle (Degree)	Max Steering Wheel Angle = 150	Steer Angle = 90

The maximum stress applied to the flexible tie rod component during simulations and testing is calculated while also a Von Mises stress contour

plot is generated in ADAMS' Postprocessor to visualize stress distribution as shown in Figures 2.3 and 2.4.

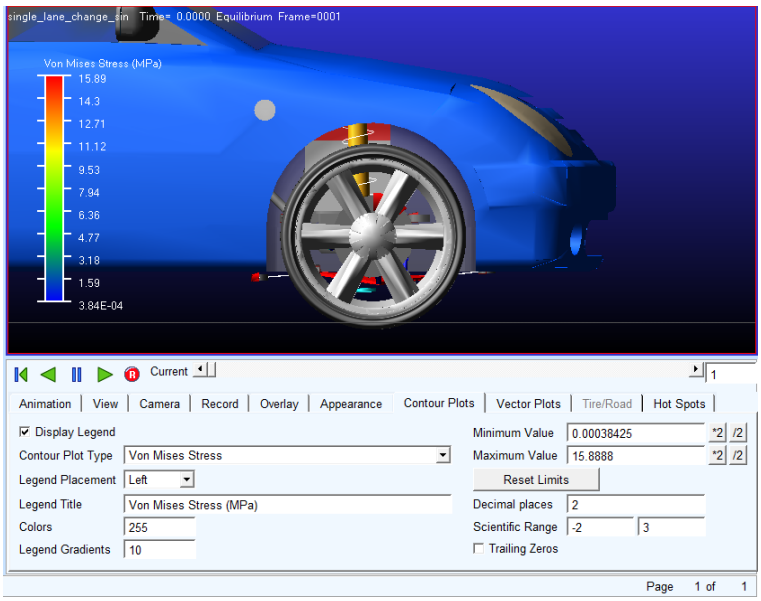

Figure 2.3. Von Mises Stress Contour Plot for Right Tie Rod During Single Lane Change

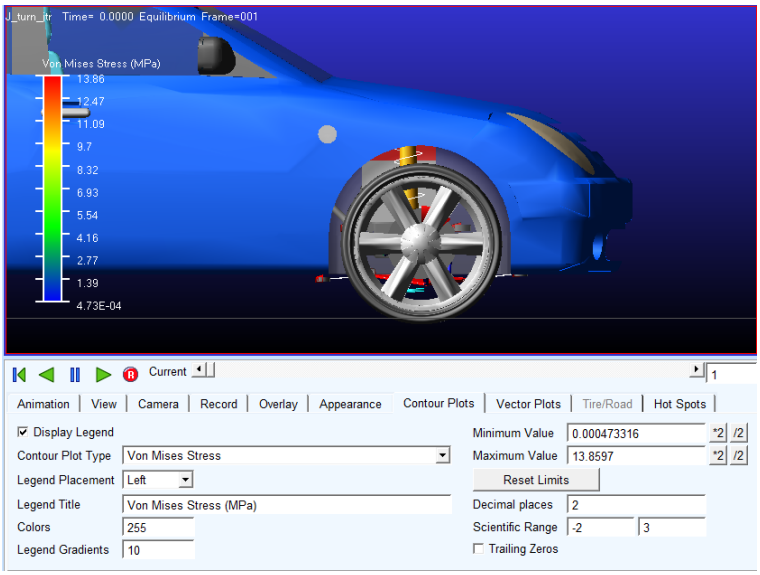

Figure 2.4. Von Mises Stress Contour Plot for Right Tie Rod During J-Turn Maneuvering

This analysis identifies peak stress concentrations and critical load zones in the tie rod under dynamic conditions, verifying whether stresses remain within the yield strength limits of the material. The results enable

structural integrity validation and inform potential design refinements if stress levels approach or exceed safe thresholds, ensuring the component meets durability requirements under extreme maneuvering loads. More details are stated in Table 2.2.

Table 2.2. Maximum Stress Values on Tie Rod

Tie Rod	Node ID	Single Lane Change Maximum Stress (MPa)	J-Turn Maximum Stress (MPa)
Right	118	15.89	13.86
Left	57	8.27	6.88

To fully evaluate the lateral dynamic behavior, the simulation must extract and analyze key handling characteristic curves including lateral velocity, roll angle, yaw rate, lateral acceleration and side slip angle. These parameters provide critical insights into the transient response of the vehicle during maneuvers, allowing engineers to assess stability, cornering performance, and overall dynamic control.

The simulations and analysis are repeated with the tie-rod modeled as a rigid component to enable direct comparison between the flexible and rigid tie-rod configurations. Subsequently, the anti-roll bar is removed from the suspension system while maintaining the rigid tie-rod assumption and the same set of curves (lateral velocity, roll angle, yaw rate, lateral acceleration, and side slip angle) are generated under these modified conditions. This two-phase comparative study satisfies the following objectives.

- Quantify the dynamic effects of tie-rod flexibility on vehicle handling characteristics

- Isolate and evaluate the specific contribution of the anti-roll bar to the roll stability and cornering behavior

The lateral velocity and acceleration curves reveal how quickly the vehicle responds to steering inputs while the roll angle indicates body lean during turns.

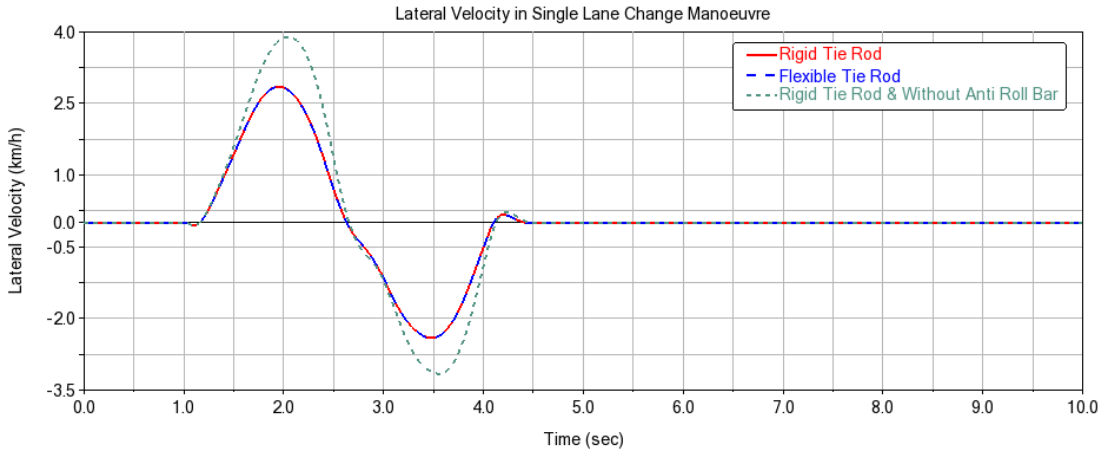

Figure 2.5. Lateral Velocity in Single Lane Change Maneuver

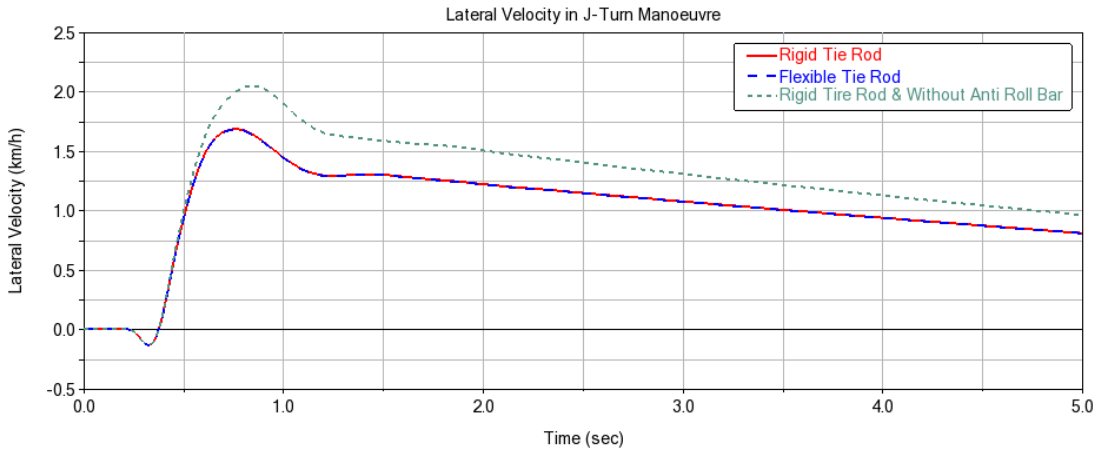

Figure 2.6. Lateral Velocity in J-Turn Maneuver

According to Figure 2.5, the lateral velocity increases when the simulation (lane changing) begins and it reaches its peak value of more than 2.5 km/h. Then it slightly falls down to the almost same speed but in the opposite direction since the lane changing is being completed. Finally, the lateral velocity gets zero when the maneuver is completed and the

vehicle becomes steady. The whole transient response is less than 4 seconds.

In J-Turn maneuvering as shown in Figure 2.6, an overshoot to more than 1.5 km/h can be seen after an insignificant undershoot and the steady behavior begins in a second.

It can be seen that the transient response is the same in the presence of flexible and rigid tie rods while the anti roll bar plays a more important role. When the anti roll bar is removed, the response amplitude increases in both simulations which can sometimes lead to instability. This emphasizes role of the anti roll bar in handling stability.

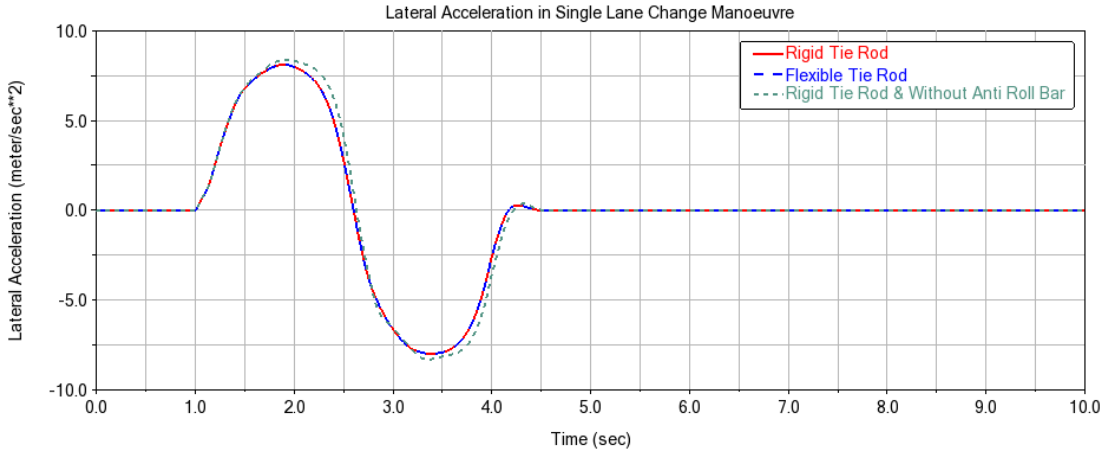

Figure 2.7. Lateral Acceleration in Single Lane Change Maneuver

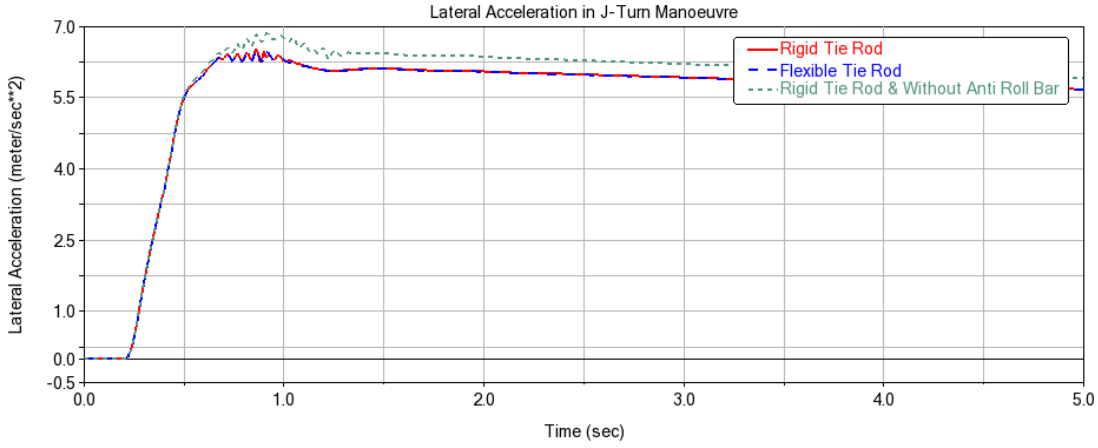

Figure 2.8. Lateral Acceleration in J-Turn Maneuver

Lateral acceleration response curves are shown in Figures 2.7 and 2.8. The general shape of these curves are similar to the lateral velocity curves. However, they are less aggressive and the effects of removing the the anti roll bar seems to have diminished.

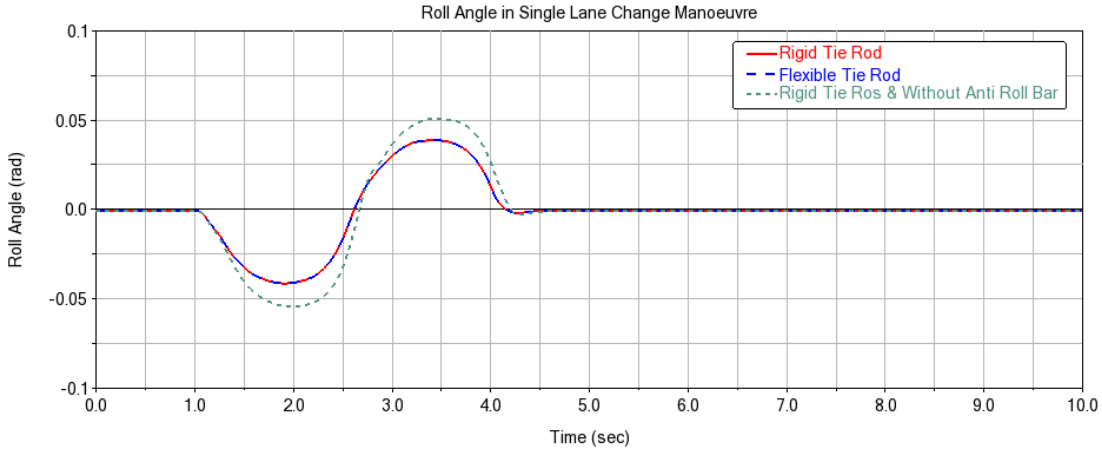

Figure 2.9. Roll Angle in Single Lane Change Maneuver

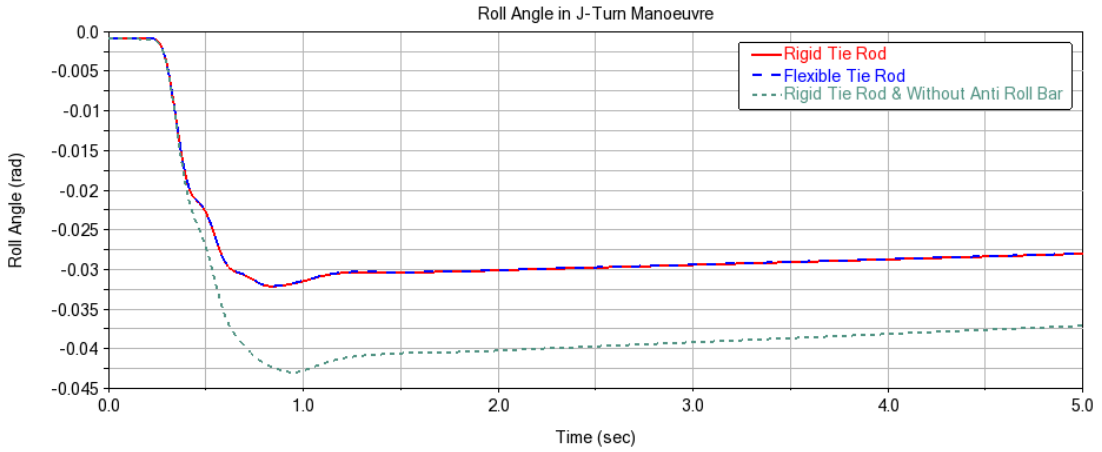

Figure 2.10. Roll Angle in J-Turn Maneuver

As mentioned, one of the most important performance characteristics in handling maneuvers, is how the vehicle rolls around its longitudinal axis. Roll angle is one of the parameters that is greatly affected by the suspension system and it makes sense that by removing the anti roll bar the vehicle would have a greater tendency to rollover especially in J-Turn maneuver as shown in Figures 2.9 and 2.10.

Yaw rate measurements quantify the rotational response of the vehicle about its vertical axis, serving as a critical indicator of directional stability during maneuvers. In standardized single lane change tests, the yaw rate curve reveals how quickly and precisely the vehicle transitions between lanes, with optimal performance showing a smooth, well-damped response that matches steering inputs (Figure 2.11). During a more aggressive J-Turn maneuver which is visualized in Figure 2.12, the yaw rate profile demonstrates the ability of the vehicle to maintain control during rapid directional changes, where excessive overshoot or slow settling may indicate instability.

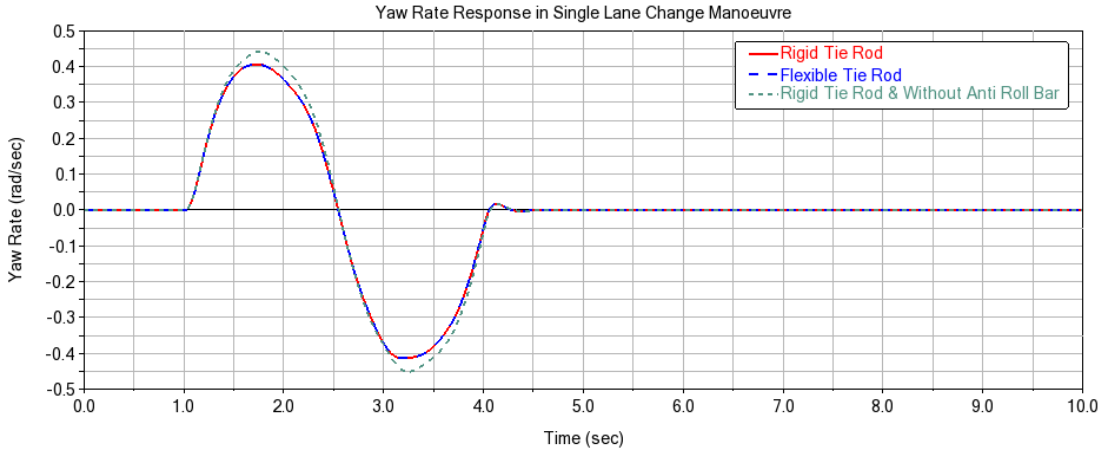

Figure 2.11. Yaw Rate in Single Lane Change Maneuver

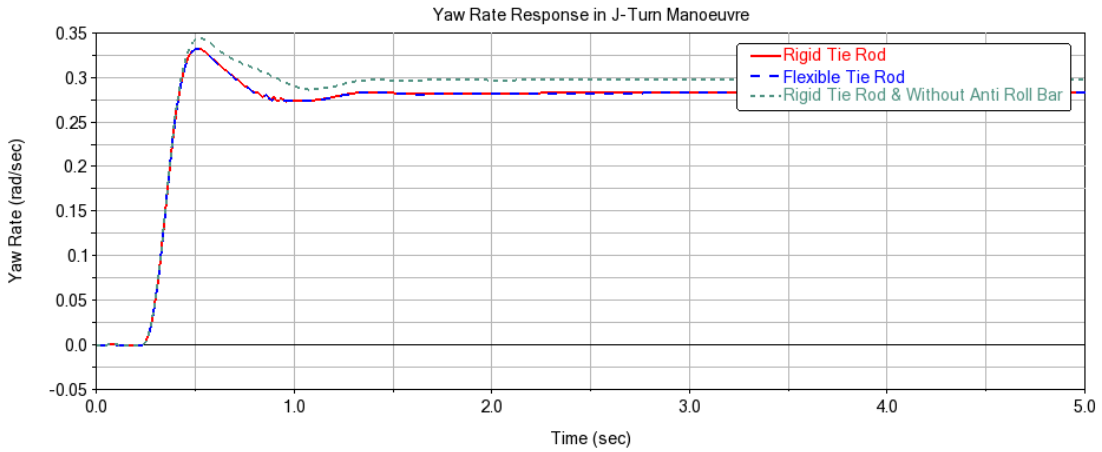

Figure 2.12. Yaw Rate in J-Turn Maneuver

Side slip angle data helps evaluate tire grip limits and stability at the limits of handling. It can be concluded from Figures 2.13 and 2.14 that the side slip angle remains within the acceptable ranges. However, removing the anti roll bar can have negative effects on tire grip and stability.

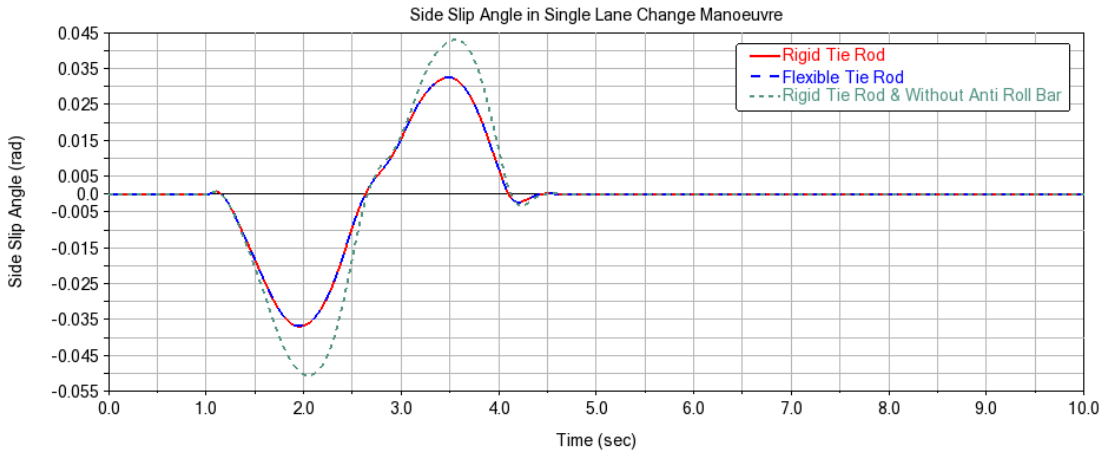

Figure 2.13. Side Slip Angle in Single Lane Change Maneuver

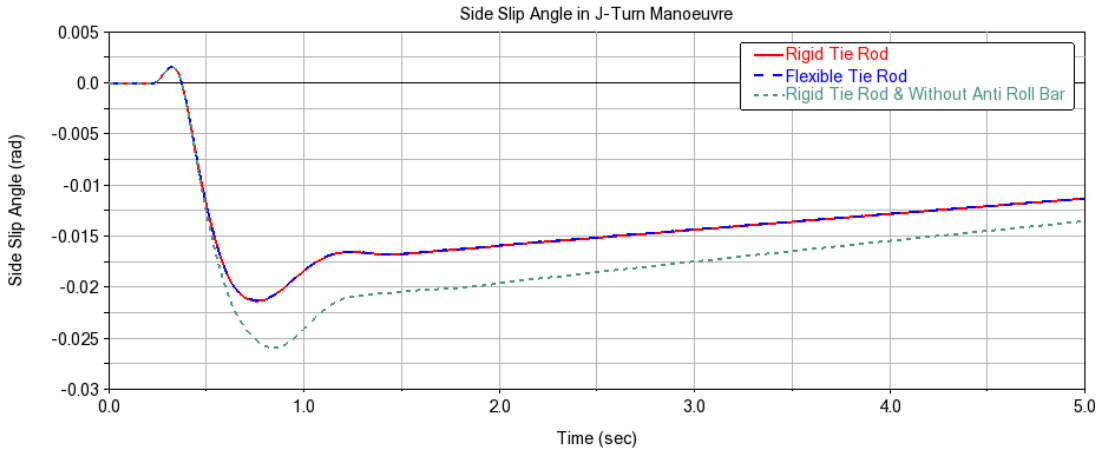

Figure 2.14. Side Slip Angle in J-Turn Maneuver

Overall, these metrics form a comprehensive picture of the vehicle dynamic performance, enabling validation against design targets and identification of potential areas for suspension or chassis refinement. The analysis of these interrelated parameters is essential for optimizing both safety and performance characteristics in the vehicle development process.

3. McPherson Suspension System Identification

The second phase of this project focuses on optimizing the front McPherson strut suspension geometry of the same AWD sedan through strategic hard-point position adjustments to enhance kinematic performance. This suspension tuning process will systematically evaluate and modify critical connection points including the strut top mount location, lower control arm pivot positions, and steering tie rod attachment points to achieve ideal camber, toe and track curves. The optimization aims to improve key handling metrics such as cornering stability, steering response, and tire contact patch consistency, with validation performed through standardized parallel wheel travel simulations that assess transient behavior under extreme maneuvers.

3.1. Baseline Simulation

First, the Suspension Assembly is created in ADAMS software environment including the suspension system, front anti roll bar and steering system as shown in Figure 3.1. In the next step, Parallel Wheel Travel analysis is performed. During this analysis, the Bump and Rebound values are set to +50 mm and −50 mm, respectively.

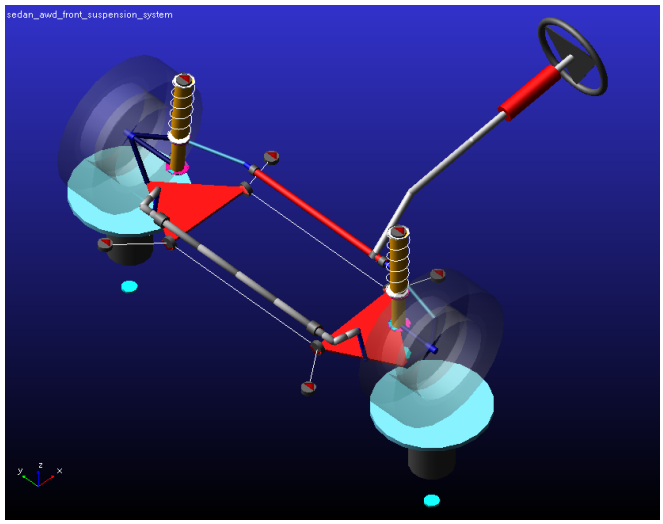

Figure 3.1. Front McPherson Suspension System with Anti Roll Bar and Steering System

Then, the Camber angle, Toe angle and Track Width alteration curves are extracted from the wheel displacement data using the Postprocessor.

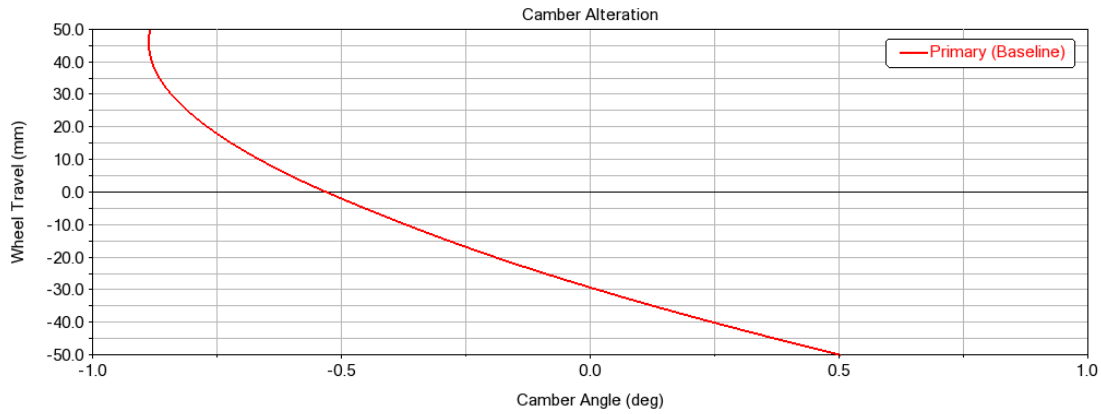

Figure 3.2. Primary Camber Alteration

A good camber alteration curve should exhibit a smooth and predictable variation, ideally maintaining negative camber during compression (bump) to enhance cornering grip. The curve should avoid abrupt changes, indicating a well-tuned suspension geometry that preserves tire contact with the road surface throughout the wheel's travel range. Minimal camber gain during rebound (which could be slightly positive) and controlled camber loss during bump help ensure consistent handling and tire wear, reflecting a balanced compromise between performance and comfort. Figure 3.2 can be better by trying to reverse the concavity of the curve and make the negative slope slower to have a larger negative camber at full bump.

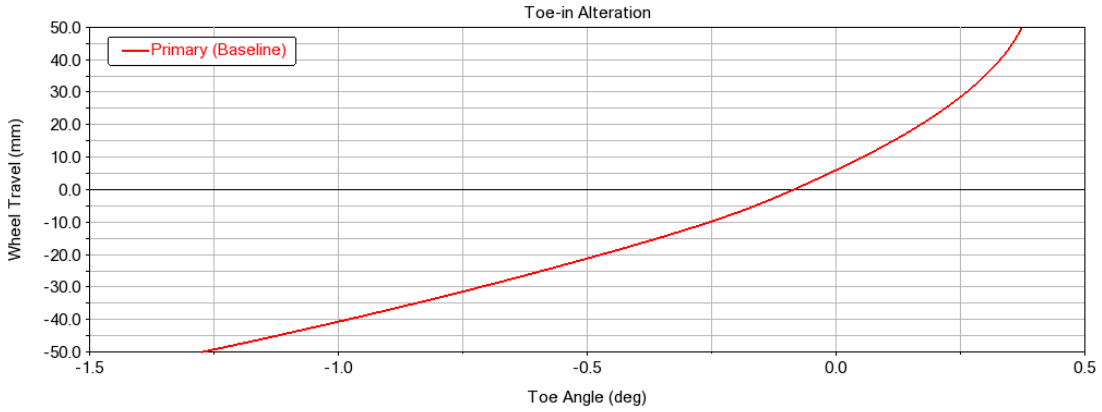

Figure 3.3. Primary Toe-in Alteration

An effective toe angle alteration curve should exhibit gradual and symmetric changes, minimizing excessive toe-in or toe-out (ideally within ±10 degrees) throughout suspension travel. This helps preserve directional stability and reduce tire scrub. Ideally, toe variation remains minimal across the wheel's range of motion, reflecting precise steering geometry and predictable handling characteristics.

During bump (typically the outer wheel in cornering), a slight negative toe angle (toe-out) is beneficial for improving grip. Conversely, under rebound (usually the inner wheel), a slight positive toe angle (toe-in) can enhance stability.

As shown in Figure 3.3, the current toe curve does not meet these performance criteria and should be revised accordingly.

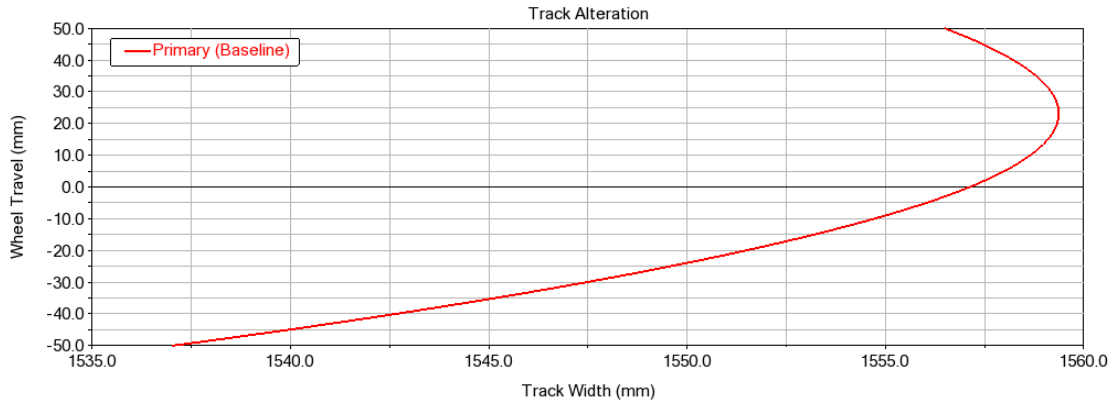

Figure 3.4. Primary Track Alteration

An increase in track width during wheel compression is a favorable kinematic trait of the suspension mechanism. As illustrated in Figure 3.4, a key limitation of the initial design is the reduction in track width under significant compression, which compromises vehicle stability during aggressive maneuvers or sharp turns. This instability arises from a substantial increase in the distance between the roll center and the center of gravity.

3.2. Sensitivity Analysis and Design of Experiments

Sensitivity Analysis in ADAMS Insight helps identify which input parameters most significantly affect system performance. By varying one parameter at a time and observing its impact on output metrics.

Design of Experiments (DOE) goes a step further by systematically exploring combinations of multiple parameters. ADAMS Insight uses DOE to build a structured set of simulations that reveal interactions between variables, enabling efficient optimization and robust design.

It is necessary to identify the 3 parameters that have the greatest impact on the mentioned curves, among the hard-points listed in Table 3.1. According to the table there are 12 candidate parameters.

Table 3.1. Candidate Design Variables

Hard-Point	x	y	z
hpl_top_mount	317.5	-580	755
hpl_lca_front	60	-400	190
hpl_lca_outer	240	-700	175
hpl_lca_rear	460	-390	205

The candidates are promoted to inclusion and the DOE is performed in ADAMS Insight using DOE Screening investigation strategy with 64

runs while the standard deviation during simulation is selected as the design objective of the sensitivity analysis. There are also other investigation methods that are briefly explained in Table 3.2.

Table 3.2. Different Investigation Strategies in ADAMS Insight

Investigation Method	Description
Study - Perimeter	Evaluates model at the extreme (min/max) values of selected variables.
Study - Sweep	Varies one or more parameters across a defined range to observe trends.
DOE Screening - 2 Level (Selected Method in this Project)	Tests each variable at two levels (high/low) to identify influential ones.
DOE Response Surface	Builds a predictive model using multiple levels to explore variable effects.
Variation - Monte Carlo	Uses random sampling to assess performance under uncertainty.
Variation - Latin Hypercube	Stratified sampling method for efficient uncertainty analysis.

After all of the experiments are designed, a HTML document is generated that contains all of the design candidates and information about the accuracy of the fitted models. Table 3.3 expresses how the models are accurate based on R2 Score and other evaluation criteria.

Table 3.3. Accuracy of Statistical Fitted Models in DOE

Response	R2 Score	R2adj	P	R/V
Camber	96.77	96.01	0	43.23
Toe	66.39	58.48	≈ 0	11.02
Track	97.36	96.74	0	45.47

Figure 3.5 illustrates main effects of the 12 candidates on response metrics. The percentage values in the last column determine how each of them are effective in alterations.

Main Effects for Response: **camber_angle**

Factor	From	To	Effect	Effect %
front_macpherson_strut_susp.ground.hpl_top_mount.y	-6.0000e+02	-5.6000e+02	2.3138e-01	54
front_macpherson_strut_susp.ground.hpl_lca_outer.z	1.5500e+02	1.9500e+02	-1.8224e-01	-42.53
front_macpherson_strut_susp.ground.hpl_lca_front.z	1.7000e+02	2.1000e+02	1.2823e-01	29.93
front_macpherson_strut_susp.ground.hpl_lca_rear.z	1.8500e+02	2.2500e+02	6.2063e-02	14.49
front_macpherson_strut_susp.ground.hpl_top_mount.z	7.3500e+02	7.7500e+02	-4.4463e-02	-10.38
front_macpherson_strut_susp.ground.hpl_top_mount.x	2.9750e+02	3.3750e+02	3.3217e-02	7.75
front_macpherson_strut_susp.ground.hpl_lca_outer.x	2.2000e+02	2.6000e+02	-2.0849e-02	-4.87
front_macpherson_strut_susp.ground.hpl_lca_outer.y	-7.2000e+02	-6.8000e+02	1.6489e-02	3.85
front_macpherson_strut_susp.ground.hpl_lca_front.y	-4.2000e+02	-3.8000e+02	-1.4037e-02	-3.28
front_macpherson_strut_susp.ground.hpl_lca_front.x	4.0000e+01	8.0000e+01	-5.3188e-03	-1.24
front_macpherson_strut_susp.ground.hpl_lca_rear.y	-4.1000e+02	-3.7000e+02	-2.9106e-03	-0.68
front_macpherson_strut_susp.ground.hpl_lca_rear.x	4.4000e+02	4.8000e+02	1.1692e-03	0.27

Main Effects for Response: **toe_angle**

Factor	From	To	Effect	Effect %
front_macpherson_strut_susp.ground.hpl_lca_outer.z	1.5500e+02	1.9500e+02	6.1013e-01	87.39
front_macpherson_strut_susp.ground.hpl_lca_rear.z	1.8500e+02	2.2500e+02	-3.2290e-01	-46.25
front_macpherson_strut_susp.ground.hpl_lca_front.z	1.7000e+02	2.1000e+02	-2.2363e-01	-32.03
front_macpherson_strut_susp.ground.hpl_lca_outer.x	2.2000e+02	2.6000e+02	1.2407e-01	17.77
front_macpherson_strut_susp.ground.hpl_lca_rear.x	4.4000e+02	4.8000e+02	-9.9344e-02	-14.23
front_macpherson_strut_susp.ground.hpl_top_mount.y	-6.0000e+02	-5.6000e+02	5.5865e-02	8
front_macpherson_strut_susp.ground.hpl_top_mount.x	2.9750e+02	3.3750e+02	3.6409e-02	5.22
front_macpherson_strut_susp.ground.hpl_lca_rear.y	-4.1000e+02	-3.7000e+02	-1.2250e-02	-1.75
front_macpherson_strut_susp.ground.hpl_lca_outer.y	-7.2000e+02	-6.8000e+02	-1.2167e-02	-1.74
front_macpherson_strut_susp.ground.hpl_top_mount.z	7.3500e+02	7.7500e+02	-8.0165e-03	-1.15
front_macpherson_strut_susp.ground.hpl_lca_front.y	-4.2000e+02	-3.8000e+02	4.3513e-03	0.62
front_macpherson_strut_susp.ground.hpl_lca_front.x	4.0000e+01	8.0000e+01	9.4517e-04	0.14

Main Effects for Response: **track**

Factor	From	To	Effect	Effect %
front_macpherson_strut_susp.ground.hpl_lca_outer.z	1.5500e+02	1.9500e+02	-2.9075	-44.31
front_macpherson_strut_susp.ground.hpl_lca_front.z	1.7000e+02	2.1000e+02	1.8022	27.47
front_macpherson_strut_susp.ground.hpl_lca_rear.z	1.8500e+02	2.2500e+02	1.3043	19.88
front_macpherson_strut_susp.ground.hpl_top_mount.y	-6.0000e+02	-5.6000e+02	3.9368e-01	6
front_macpherson_strut_susp.ground.hpl_lca_outer.y	-7.2000e+02	-6.8000e+02	2.5968e-01	3.96
front_macpherson_strut_susp.ground.hpl_lca_front.y	-4.2000e+02	-3.8000e+02	-2.2244e-01	-3.39
front_macpherson_strut_susp.ground.hpl_lca_outer.x	2.2000e+02	2.6000e+02	-1.4610e-01	-2.23
front_macpherson_strut_susp.ground.hpl_lca_rear.y	-4.1000e+02	-3.7000e+02	-1.0733e-01	-1.64
front_macpherson_strut_susp.ground.hpl_top_mount.z	7.3500e+02	7.7500e+02	-7.7491e-02	-1.18
front_macpherson_strut_susp.ground.hpl_lca_rear.x	4.4000e+02	4.8000e+02	-7.0419e-02	-1.07
front_macpherson_strut_susp.ground.hpl_lca_front.x	4.0000e+01	8.0000e+01	-6.2989e-02	-0.96
front_macpherson_strut_susp.ground.hpl_top_mount.x	2.9750e+02	3.3750e+02	5.8574e-02	0.89

Figure 3.5. Main Effects of the Candidates

According to Figure 3.5, 3 design parameters with the greatest impact are listed in Table 3.4 and the optimization can be done by adjusting these parameters.

Table 3.4. Selected Design Parameters for Optimization

Factor (Parameter)	Absolute Effect on Camber (%)	Absolute Effect on Toe (%)	Absolute Effect on Track (%)
hpl_top_mount.y	54	8	6
hpl_lca_outer.z	42.53	87.39	44.31
hpl_lca_front.z	29.93	32.03	27.47

4. Optimization using Neural Networks and Gradient Based Methods

This chapter presents a data-driven approach for optimizing the discussed performance curves. By integrating simulation data from ADAMS Insight with machine learning techniques, the chapter aims to improve camber, toe and track behavior under wheel travel.

The idea is to fit a meta-model (e.g., polynomial or neural network) to predict camber/toe (track is ignored in optimization but it is coupled with camber and toe) from hard-points. Then Optimizing the meta-model to find hard-points that minimize error or the cost function is desired. The technical coding parts of this chapter is implemented using Python programming language and its useful libraries.

4.1. Dataset Collection

The process begins with feature engineering driven by the Design of Experiments (DOE) framework obtained earlier, which systematically varies key hard-points to explore their influence on suspension behavior. This structured approach generates a comprehensive dataset of 8,000 rows, enabling effective sensitivity analysis and serving as the foundation for predictive modeling. The resulting CSV file includes both input features and output parameters as illustrated in Figure 4.1. The dataset is collected using Python and Pandas library.

	hpl_top_mount.y	hpl_lca_outer.z	hpl_lca_front.z	camber_angle	toe_angle	track
0	-600.0	155.0	170.000000	0.339787	0.476949	6.916914
1	-600.0	155.0	172.105263	0.346536	0.465179	7.011769
2	-600.0	155.0	174.210526	0.353286	0.453409	7.106624
3	-600.0	155.0	176.315789	0.360035	0.441638	7.201479
4	-600.0	155.0	178.421053	0.366784	0.429868	7.296333
...	...	...	...	...	...	...
7995	-560.0	195.0	201.578947	0.490170	0.966378	5.825936
7996	-560.0	195.0	203.684211	0.496919	0.954608	5.920790
7997	-560.0	195.0	205.789474	0.503669	0.942838	6.015645
7998	-560.0	195.0	207.894737	0.510418	0.931068	6.110500
7999	-560.0	195.0	210.000000	0.517167	0.919297	6.205354

Figure 4.1. Dataset

4.2. Preprocessing

After feature engineering, data collection and cleaning, it is necessary to perform a preprocessing stage on it. For this purpose, the data is normalized and scaled and is ready for use for training the model. Using Python and Sci-kit Learn library data is normalized by StandardScaler function and is divided into training and test sets (80/20).

4.3. Model Training and Evaluation

A multi-layer perceptron (MLP) regressor neural network with two hidden layers (100, 50 neurons), ReLU activation and Adam optimizer is trained using Sci-kit Learn to map hard-point configurations to camber and toe outputs. The model achieves high accuracy with the R^2 of 0.998 on both train and test sets, enabling reliable predictions as shown in Figures 4.2 and 4.3. After the camber/toe angles are obtained, they are mapped to the corresponding wheel travel using fitted cubic functions extracted from Figures 3.2 and 3.3.

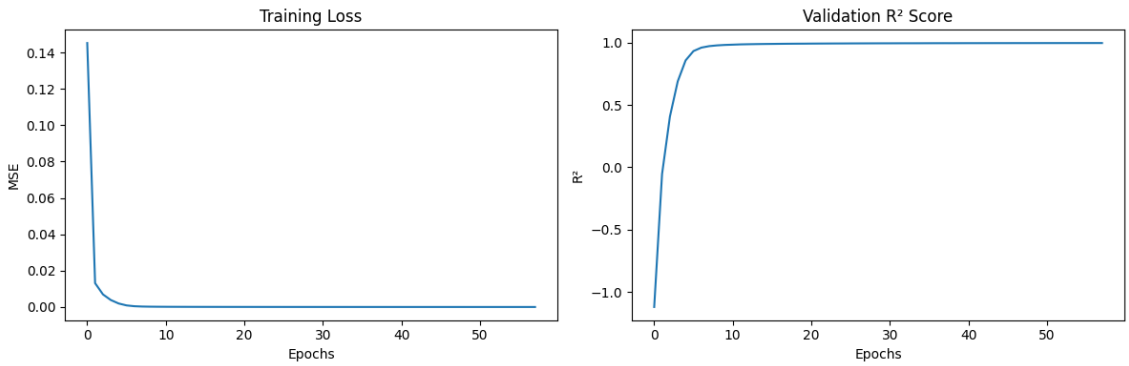

Figure 4.2. Mean Squared Error and Accuracy (R Score) vs Epochs for Validation Data

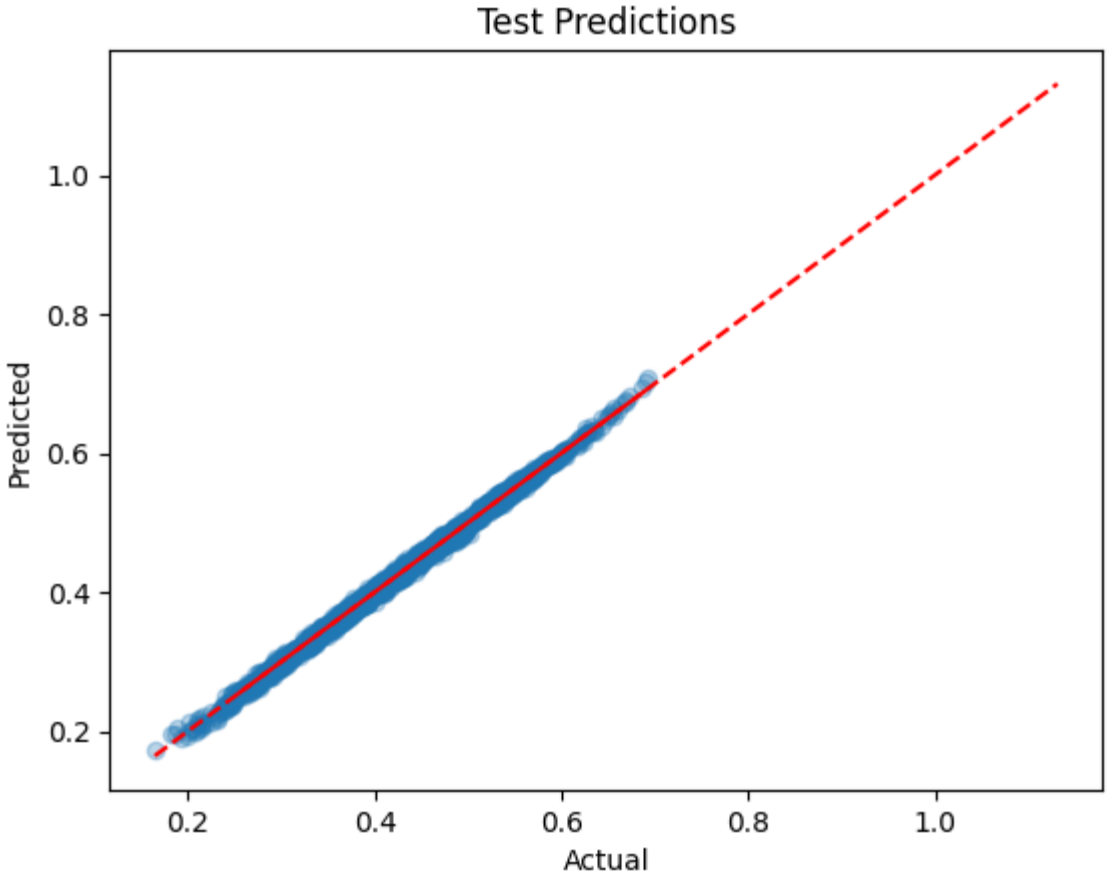

Figure 4.3. Evaluation Result for the MLP Regressor

4.4. Optimization

Target camber and toe curves are defined to reflect ideal suspension behavior during bump and rebound. These serve as objective functions for optimization. Table 4.1 shows ideal (target) values for 5 different cases of full rebound, mid-cornering rebound, static, mid-cornering bump and full bump. These values are selected based on vehicle class.

Table 4.1. Target Camber and Toe Angles

Wheel Travel (mm)	Camber (degree)	Toe (degree)
-50 (Full Rebound)	0.5	0.1
-25 (Mid Rebound)	0.2	0
0 (Static)	-1.2	0.05
25 (Mid Bump)	-1.9	-0.1
50 (Full Bump)	-2.1	-0.16

Different curves are fitted on the target values and the best models are cubic polynomials with R Score > 0.99 as shown in Figures 4.4 and 4.5.

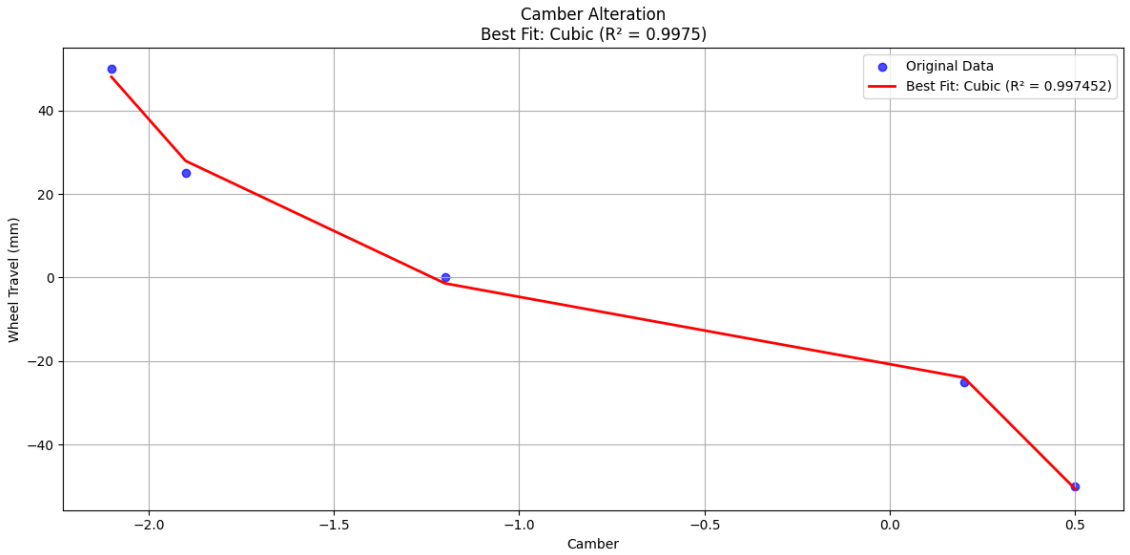

Figure 4.4. Target (Objective) Camber Curve

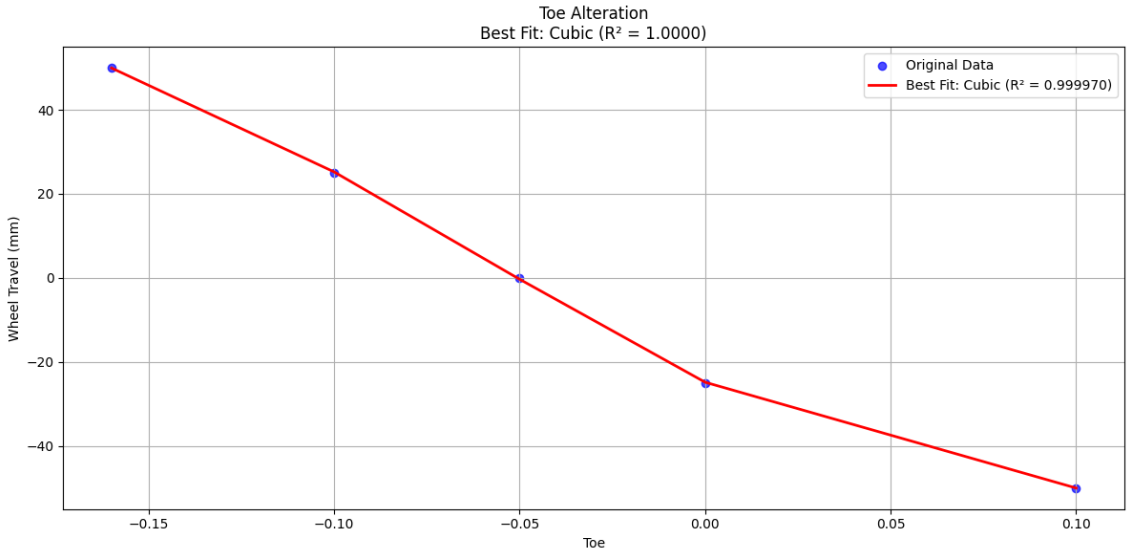

Figure 4.5. Target (Objective) Toe Curve

The same regression algorithms are implemented using Scipy library on actual curves in Figures 3.2 and 3.3 and it can be seen from Figures 4.6 and 4.7 that the cubic function is again the best fitted model with accuracy of more than 0.99. all of these fitted cubic functions are expressed in Equations 4.1-4.4.

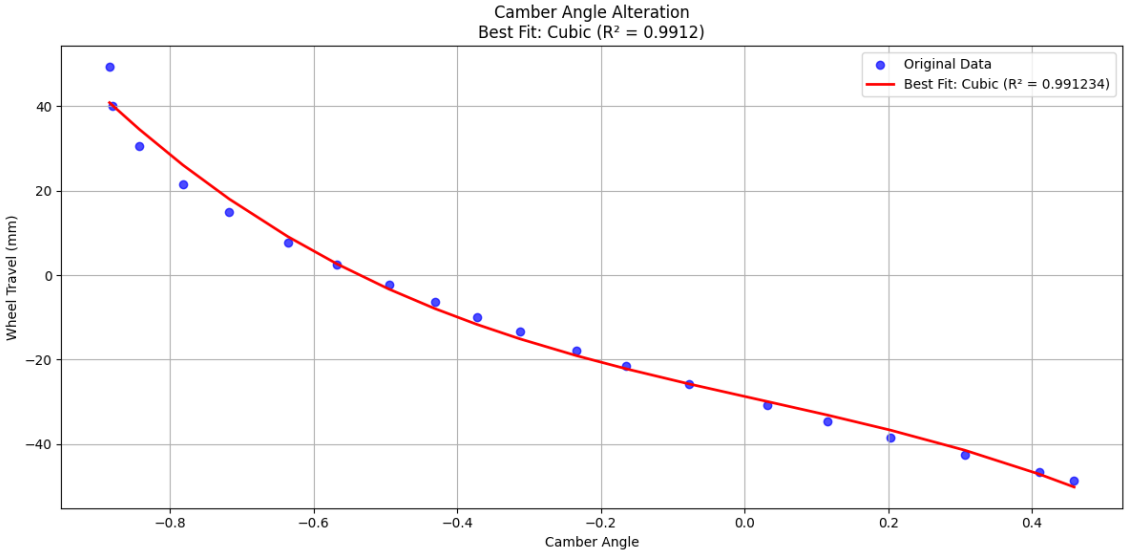

Figure 4.6. Actual (Current) Baseline Camber Curve

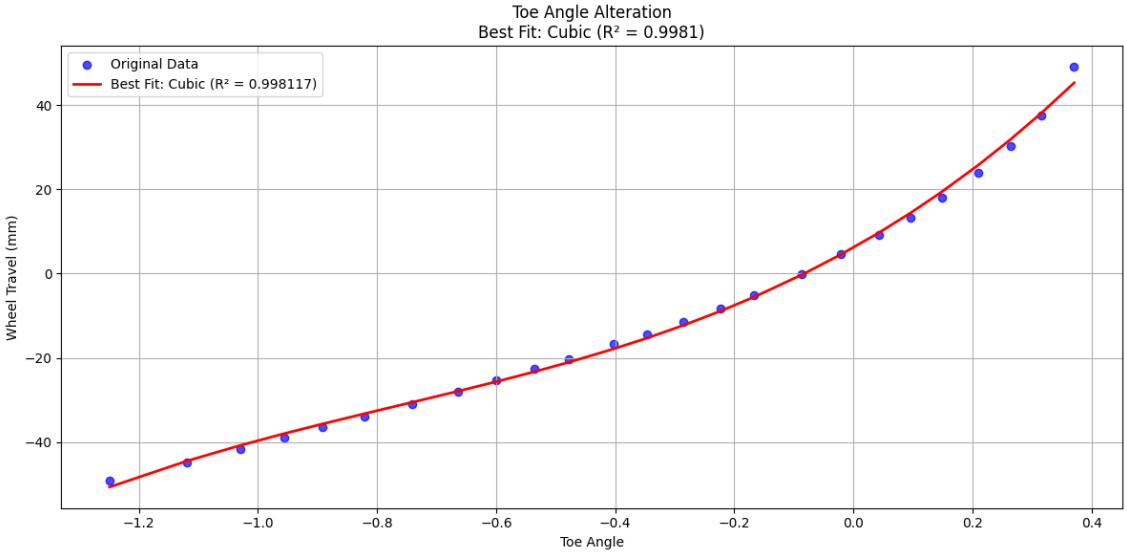

Figure 4.6. Actual (Current) Baseline Toe Curve

$$s(\epsilon) = -48.76258113x^3 + 3.03680145x^2 - 37.87645218x - 28.72789553$$ (Equation 4.1)

$$s(\delta) = 26.12141996x^3 + 59.97397949x^2 + 79.71489359x + 6.19447021$$ (Equation 4.2)

$$s(\epsilon) = -22.96634834x^3 - 54.31766864x^2 - 41.96792673x - 13.22145237$$ (Equation 4.3)

$$(\delta) = 6908.21532205x^3 + 1243.58113283x^2 - 445.28034159x - 24.83310947$$ (Equation 4.4)

Where ε is the camber angle, δ is the toe angle and s is the wheel base function.

Therefore, the objective or the cost function in this case, can be obtained from the difference between current (actual) and target curves over a range of wheel travel (squared error) as shown in Equation 4.5-4.7.

$$E_{\text{camber}} = \sum \left(s_{\text{current}}(\varepsilon) - s_{\text{target}}(\varepsilon) \right)^2$$ (Equation 4.5)

$$E_{\text{toe}} = \sum \left(s_{\text{current}}(\delta) - s_{\text{target}}(\delta) \right)^2$$ (Equation 4.6)

$$E_{total} = E_{camber} + E_{toe}$$ (Equation 4.7)

Physical bounds for hard-points should also be defined as optimization constraint and scaled for optimization. These hard-points are only allowed to move ±20 mm in each direction.

Finally, the objective (cost) function is ready to be minimized in the presence of scaled constraints. There are many optimization algorithms that can be used to solve this problem. Table 4.2 demonstrates some of the famous Gradient-Based methods.

Table 4.2. Optimization Methods Comparison

Method	Type	Gradient Use	Constraints Handling	Scaling
L-BFGS-B (Selected in this Project)	Quasi-Newton	Approximates Hessian	Yes	Efficient for Medium-Scale Problems
Gradient Descent	First Order	Uses Exact Gradient	No	Simple, Slower Convergence
Adam	Stochastic GD	Adaptive Moments	No	Great for NNs

Based on the project requirements, Limited-Memory Broyden-Fletcher-Goldfarb–Shanno with Box constraints (L-BFGS-B) is preferred. This algorithm is a Quasi-Newton method, which is a second-order optimization technique that uses gradient information to approximate the Hessian (second derivative matrix). It is in the same family with Gradient Descent yet smarter and more efficient, especially for problems with bounded variables and nonlinear loss functions same as this problem.

The optimization algorithm is executed in Python and Scipy to find hard-point positions that best match the target curves, while respecting physical constraints. The obtained optimized design parameters are shown in Table 4.3.

Table 4.3. Optimized Design Parameters

Factor (Parameter)	Optimized Value
hpl_top_mount.y	-599.93
hpl_lca_outer.z	155
hpl_lca_front.z	207.26

Finally, the hard-points are adjusted according to the optimized values and the corresponding modified curves are plotted in Figures 4.8-4.10. To get a better vision of the improved suspension performance, the relevant baseline and target camber/toe curves are also illustrated in Figure 4.7.

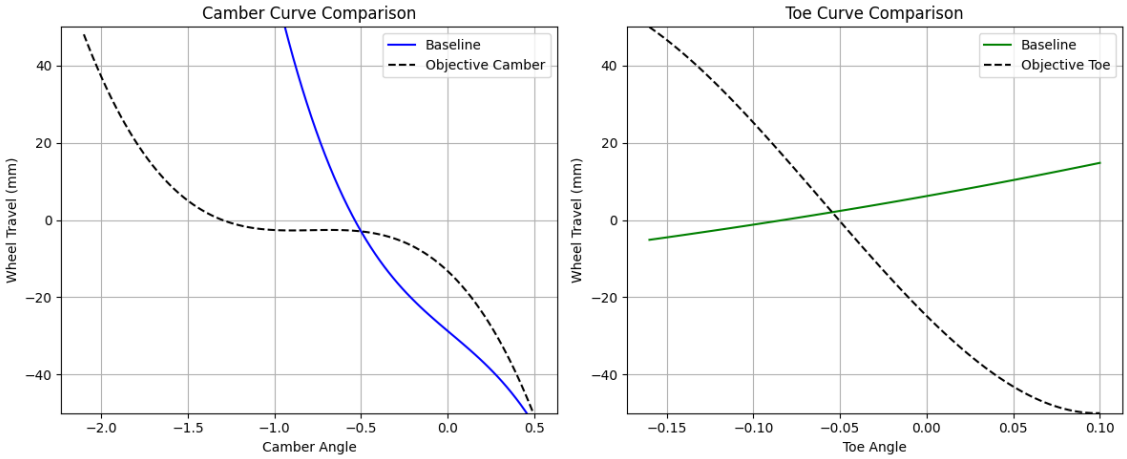

Figure 4.7. Comparison of the Baseline and Target Camber and Toe Curves

As illustrated in Figure 4.8, the modified model exhibits increased negative camber under compression during maneuvers or turns. This enhances camber thrust and lateral force on the outer wheel, contributing to improved lateral stability of the vehicle. It more closely aligns with the target curve while still having the kinematic limitations of a McPherson suspension system.

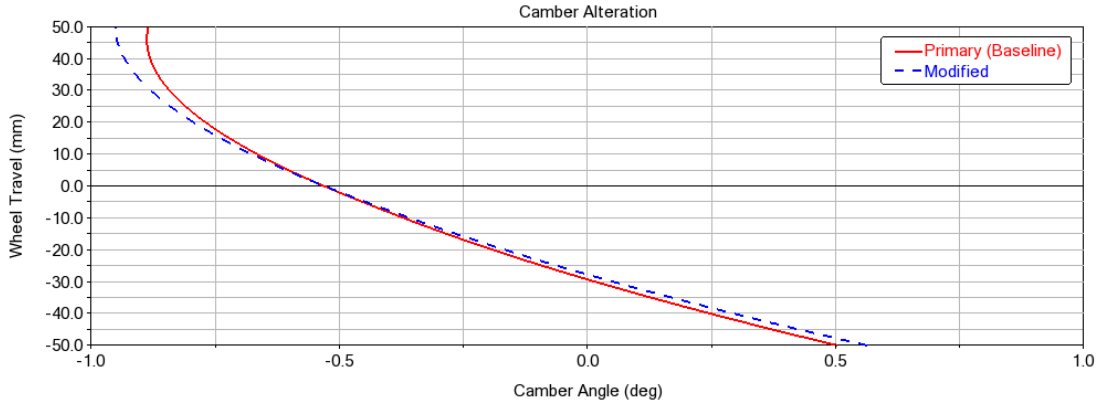

Figure 4.8. Comparison of the Baseline and Modified Camber Alteration

Figure 4.9 illustrates the changes in toe angle, which play a key role in the roll-induced understeering behavior. The figure indicates that after optimization, the understeer gradient of the model has been reduced. While increased understeer generally enhances vehicle stability during maneuvers, it can compromise steer-ability. This trade-off explains why the target curve was designed with a lower understeer gradient than the initial model (which was more likely to be oversteer). As a result, the modified mechanism enables a quicker response to the driver's steering input.

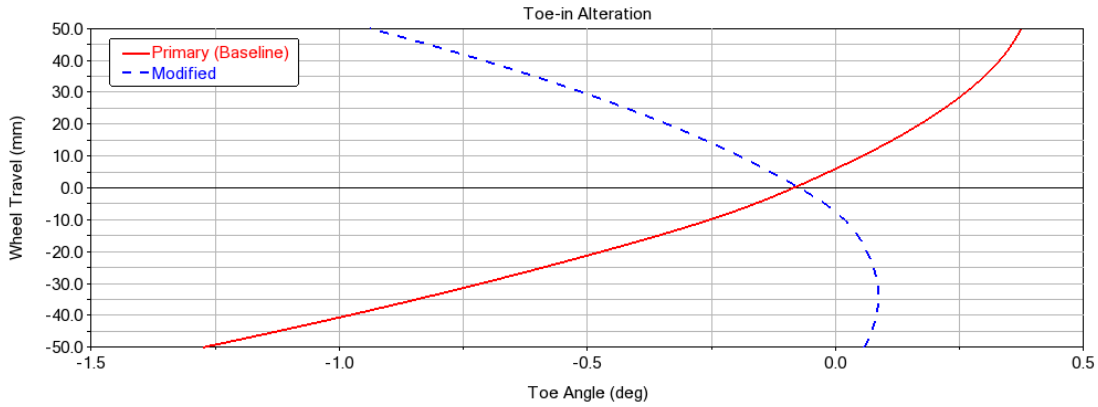

Figure 4.9. Comparison of the Baseline and Modified Toe-in Alteration

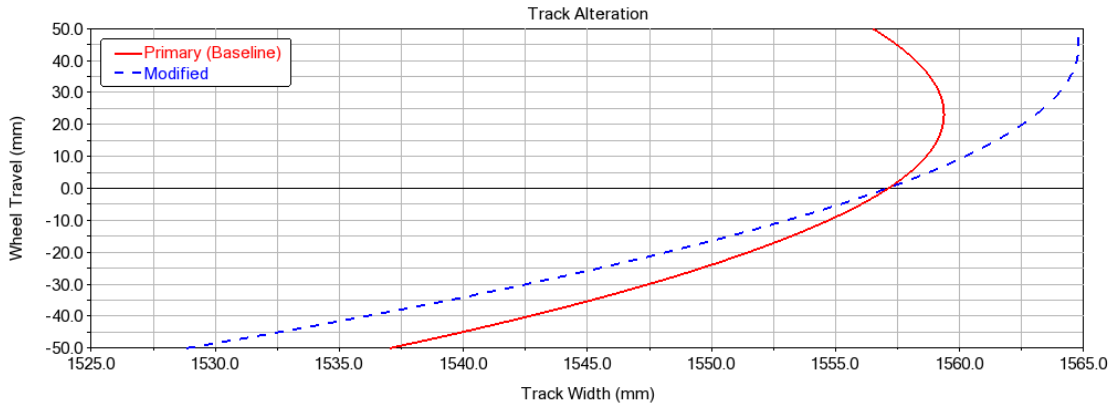

Figure 4.10. Comparison of the Baseline and Modified Toe-in Alteration

An increase in track width during wheel compression enhances the kinematic performance of the suspension mechanism. As shown in Figure 4.10, a key drawback of the initial model is the reduction in track width when the wheel compresses beyond 50 mm. This poses a significant risk to

vehicle stability during aggressive maneuvers or sharp turns, as excessive compression increases the distance between the roll center and the center of gravity. Although the focus of the optimization was not on the track, the modified mechanism almost eliminates this issue.

Conclusion

The study successfully integrates machine learning and gradient-based optimization techniques to enhance the kinematic performance of a McPherson suspension system. Through systematic sensitivity analysis and DOE, critical hard-points were identified and optimized, resulting in improved camber and toe curves that align with target performance metrics. The neural network model demonstrated high predictive accuracy, enabling efficient optimization with the L-BFGS-B algorithm. The final design achieved better lateral stability, reduced understeer, and minimized track width deviations, addressing key limitations of the baseline suspension. This approach not only validates the effectiveness of data-driven optimization in suspension design but also provides a scalable framework for future advancements in vehicle dynamics engineering. The findings underscore the potential of combining simulation, machine learning, and optimization to achieve superior suspension performance in automotive applications.

References

[1] Jornsen Reimpell, Helmut Stoll and Jurgen W. Betzler, “The Automotive Chassis: Engineering Principles”, Butterworth-Heinemann, 2001.

[2] N. Ikhsan, R. Ramli and A. Alias, “Suspension Optimization Using Design of Experiment (DOE) Method on MSC/ADAMS-INSIGHT”, *Jurnal Teknologi*, August 2015.

[3] Lijun Qian and Qin Shi, “Optimization of Wheel Positioning Parameters of Automotive Front Suspension Based on ADAMS”, School of Mechanical and Automotive Engineering, HeFei University of Technology, China.

[4] Du Canyi, Zhu Baochai, Wang Hengbo, Mai Xingye and Qin Taixing, “Design and Optimization of Front Suspension of FSAE based on ADAMS Simulation”, 4th International Conference on Sensors, Mechatronics and Automation, 2016.

[5] Sayyad Nasiri, Naser Sina and Abolqasem Eslami, “Multi-objective Optimisation of McPherson Strut Suspension Mechanism Kinematics using Random Search Method”, *Indian Journal of Science and Technology*, July 2015.